UCRL-91836 Rev. 1
PREPRINT

DYNAMIC COMPACTION OF ALUMINUM NITRIDE POWDER: HUGONIOT MEASUREMENT AND COMPARISON WITH STATIC BEHAVIOR

W. H. Gourdin
S. L. Weinland

This paper was prepared for submittal to
Journal of the American Ceramic Society

June 25, 1985

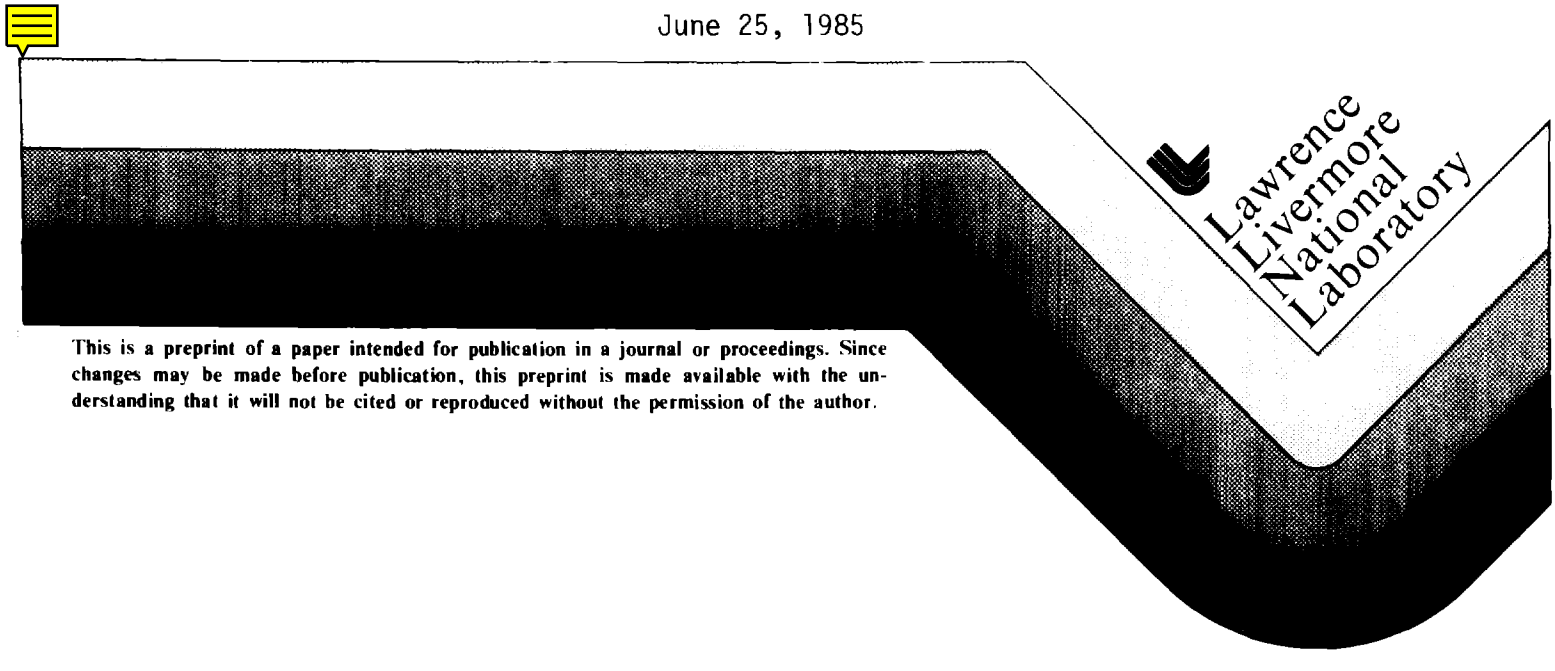

DISCLAIMER

DYNAMIC COMPACTION OF ALUMINUM NITRIDE POWDER: HUGONIOT MEASUREMENT AND COMPARISON WITH STATIC BEHAVIOR*

W. H. Gourdin

S. L. Weinland

Lawrence Livermore National Laboratory

University of California, Livermore, California 94550

Abstract

We have performed a limited number of shock Hugoniot measurements for two unsintered aluminum nitride powder compacts having initial densities of 1.30 g/cm^3 and 1.53 g/cm^3. Stresses achieved in our experiments range from 0.25 to 1.8 GPa, corresponding to linear compaction rates of 0.3 to 0.6 km/s. We find that densification is incomplete behind the first shock wave, proceeding only to about 70% of the solid density regardless of the initial density. Upon reshock, however, significantly higher densities are achieved. Initial compaction of the powder to a relative density of 65 to 70% occurs readily at stresses below 0.25 GPa. For greater stresses, however, densification is slight. Comparisons with static compression data on the same powders suggest that this resistance to compaction is an effect of compaction rate.

---

* Work performed under the auspices of the U.S. Department of Energy by the Lawrence Livermore National Laboratory under Contract W-7405-ENG-48.

I. Introduction

The static compaction behavior of ceramic powders has been the subject of several studies.[1-6] Some recent work, however, has explored the dynamic, or shock wave, compaction of ceramic powders, both as a technique for the production of fully dense, well-bonded materials[7-12] and as a means of inducing high-pressure and high-temperature phase changes.[13-15] The analysis of the dynamic experiments rests in large part on a knowledge of the shock response of the powders under study, for it is from the locus of states achieved upon shock loading, the Hugoniot curve, that the densities and energy densities behind the various shock waves are deduced. The latter quantity is of particular concern, as it determines the type and extent of local microstructural changes in the powder.[16] Hugoniot data for a number of porous ceramics are given in Ref. 17. Some data for silicate minerals are also available in the geophysical literature,[18-19] applied to the interpretation of impact and high-pressure wave-propagation phenomena. Information on technical ceramics, however, is in large part restricted to high stresses, in excess of 10 GPa,[17,20,21] which are suitable for equation-of-state determinations but may be greater than needed merely to achieve full density or adequate cohesion. Some data at lower pressures are available for MgO and Al_2O_3.[21,22]

Aluminum nitride undergoes a brittle-to-ductile transition when loaded triaxially,[23] and shows considerable plasticity during dynamic compaction.[9-11] Its dynamic properties are thus of particular interest. In this paper, we present our measurements of the Hugoniots of two aluminum nitride powders having different initial packing densities. These experiments are limited in number, and we do not claim them to be definitive. They do, however, indicate the general behavior of these materials under dynamic loading. We first describe our experiments and starting materials. We then

present our results and analyze them to show that complete densification is not achieved upon passage of the initial shock, and that reflections of the initial shock ("reshock") produce significant increases in the compact density. The variation of density with dynamic stress is presented and discussed in relation to static compression data. We note in particular what appear to be compaction-rate effects. A detailed discussion of the experiments and error analysis is included in the Appendix.

II. Experimental Procedure

The experiments in this study were conducted with a helium-driven 6.35-cm-bore light gas gun. Aluminum 6061 projectiles of various weights were used, and the projectile speed could be varied up to a maximum of 800 m/s. Projectile speed was determined to within 1 to 2% using a system of electrically shorting whisker pins placed in the muzzle just in front of the sample.

The sample was positioned at the end of the muzzle in the assembly shown schematically in Fig. 1. The powder was packed by means of a vibrator into the 0.2-cm gap between a 0.3-cm-thick cover plate and a 1.27-cm-thick back plate (both of aluminum 6061). The use of the same material for projectile and cover produces a single, well-defined shock in the powder, simplifying the analysis.* The high aspect ratio of the arrangement insured that this shock was one-dimensional near the center of the sample. Thin-film carbon

---

* Although the initial loading of the powder is complex, a single shock forms after a brief "shock-up" period, as discussed in the Appendix.

piezoresistive shock pressure sensors* were affixed with a thin film ($\lesssim$0.0013 cm) of epoxy to the cover and back plates (Fig. 1) such that the 0.15 X 0.13 cm active elements were on the central axis. These sensors were used to record the initial shock stress and the reshock stress in the compact. However, primary emphasis was placed on measurements of shock transit time and impedance matching[24] in determining the shock states of the powder, because of their freedom from calibration errors. The transit time between the two carbon sensors was measured directly, and the thickness of the specimen was taken to be the distance between the midplanes of the sensors. Measured rise times were restricted by the reverberation time with the sensor to 100-200 ns or longer. The relative tilt of the sample and projectile at impact was measured with three piezoelectric sensing pins spaced equally around the rim of the cover. Because of the small size of the piezoresistive elements and their placement on axis, the relative tilt, typically 2.5 mrad, had no significant effect upon our measurements. All experiments were conducted in a vacuum of 100 millitorr or less. Further details of these experiments are given in the Appendix.

The hydrostats of the powders were obtained using the method discussed in Ref. 25. Samples were sealed in cylindrical tin containers 1.27 cm in diameter by 2.54 cm in length and compressed in a piston-cylinder die, end-loaded in a double-acting press.[25] The very low yield strength of the tin produces conditions which are very nearly hydrostatic, and the sample

---

* Dynasen, Inc., Goleta, CA. The change in resistance of these sensors with stress is measured with a bridge circuit, of which it forms one leg. The voltage across the bridge is recorded on an oscilloscope, and with suitable calibration this voltage - time record may be converted directly to a stress - time history.

compression at pressure can be deduced from the ram displacement. Corrections for die distortion and friction are obtained from separate experiments on a solid nickel standard. The relatively large size of the static specimens compared with the 0.2-cm-thick samples used in the dynamic measurements produced higher initial packing densities in the static experiments (1.96 g/cm^3, 60%, for powder I; 1.79 g/cm^3, 55%, for powder II).

Aluminum nitride powders were obtained from two different commercial sources, and the properties of each powder are summarized in Table I. The particles of powder I consist of micrometer-sized agglomerates of $\sim$0.1-μm crystallites, as shown in the micrograph of Fig. 2. Powder II has a similar character. Neither powder is pure, but the 4-6% contamination (principally oxides or oxy-nitrides) is typical and is expected to have little effect on their dynamic response.

III. Results

A representative sensor record is shown in Fig. 3. The initial stress in the powder, at the front sensor (Fig. 3a), rises within 160 ns to a peak and then relaxes to a plateau. The peak is probably a capacitive effect common to sensors of the type used here,[26] but may also be related to the porosity of the specimens. The value of the stress at the plateau was in all cases taken to represent the stress in the compacted powder behind the initial shock front. This stress remains constant until the return of the reflected wave, showing that lateral release does not occur in the center of the specimens in the time span of interest here, and that the initial compaction occurs under average conditions of one-dimensional strain. Conditions behind the initial shock are summarized in Tables II and III.

The reshock stress, reflected at the back of the assembly (Fig. 3b), rises rapidly to a much higher level than the initial shock. The reshock

stresses given in Tables II and III have been corrected for errors in calibration, which have been reported for these sensors at stresses in excess of about 2.0 GPa.[27] The records provide no clear evidence for a lower-amplitude stress wave that precedes the main compaction shock ("precursor"), such as observed in experiments with pressed or sintered porous metals.[28,29] We attribute this to the low density and lack of cohesion of the initially unsintered powder. It should be noted, however, that the resolution of our measurements is limited to 100 to 200 ns by the sensor thickness.

The Hugoniot curves we obtained for the two powders are shown in the stress - material speed plane in Fig. 4. We find satisfactory agreement between the impedance-matching results and the direct sensor measurements in the stress range produced by the initial shock, in accord with previous work.[27] Also shown in Fig. 4 are the states achieved upon reshock, all of which necessarily lie along the Hugoniot of the aluminum 6061 back plate.[24] The slopes of the reshock Rayleigh lines are significantly less than that of solid AlN.

No attempt was made to examine material recovered from these experiments. Material recovered from similar experiments, however, showed that the compacts were badly fractured and had little strength. The densities of these specimens, as determined by mercury porosimetry, ranged from 79% to 85% of the solid. These densities are in accord with those derived from Hugoniot data in the following section.

IV. Analysis

The presentation of the Hugoniot in the plane of the stress, P, and the average material speed behind the shock, U_p, is particularly convenient because these data are obtained directly from both the sensor and the

impedance-matching measurements. The Rankine-Hugoniot relationships, however, relate P and U_p to the shock speed, v_s, and the specific volume, V, so that given any two of these variables, the other two may be calculated. These relationships are derived and discussed extensively elsewhere[24] and are summarized briefly for convenience in the Appendix.

Equation (A-4) may be used directly to determine the specific volume behind the shock, or we can combine Eqs. (A-1) and (A-2) to yield

$$(U_p - U_0)^2 = (P - P_0)(V_0 - V) \quad , \tag{1}$$

where the subscripts denote the initial states in front of the shock. For the initial shock, $U_0 = 0$ and $P_0 = 0$, so that Eq. (1) reduces to:

$$V = V_0 - \frac{U_p^2}{P} \quad . \tag{2}$$

The specific volumes and densities (1/V) derived from Eqs. (1) and (2) are collected in Tables II and III, and the relative densities from impedance matching only are plotted as a function of stress in Fig. 5. Within the stress range studied there is relatively little change in the density of the compact behind the initial shock. It should be noted that these are the densities at the stress indicated, and as such differ from the usual values quoted for compacted powders after the stress has returned to ambient. They do not, therefore, include increases in the specific volume which may occur as a result of pore or crack opening during release. The large error bars shown in Fig. 5 result from the dependence of V on the square of the material speed and the inverse of the stress in Eqs. (1) and (2). A relatively modest error in these quantities translates into a substantially larger error in the calculated specific volume.

The densities given in Table II and III show that complete consolidation is not achieved behind the initial shock. This is apparent from the

comparison in Fig. 4 of the experimental Hugoniot curves and those derived assuming that complete densification of the powder occurs regardless of stress. Significant increases in density also occur upon reshock, although these are not sufficient to fully consolidate the powder.

A least-squares analysis of the data for the 1.53-g/cm^3 powder, which shows the least scatter, yields a linear relationship between the stress and the relative specific volume of the powder:

$$\rho_r = V_{solid}/V = 0.685 + 0.017P \quad , \tag{3}$$

where P is in GPa. This relationship may be used in a description of the dynamic compaction of porous materials[30,31*] to produce the curves indicated in Figs. 4 and 5. There is little statistical significance to Eq. (3), however, and data for both initial densities can be equally well described by a constant value of 0.70.

This behavior contrasts with the static compression curves, also shown in Fig. 5. These are typical of ceramic powders, and show a relatively large initial slope, $d\rho/dP$, which decreases quickly and continuously as the pressure and density increase. Within the range studied, the initial density has little effect on the static high-pressure behavior of the powder.

---

* These models actually describe the powder consolidation in terms of a P-α relationship in which α is the ratio V/V_{solid}, where V_{solid} is the volume of the solid at the stress specified. This is slightly less than the solid specific volume under ambient conditions, but at the low stresses considered here the difference is negligible.

V. Discussion

The reshock states summarized in Tables II and III and shown in Fig. 4 are determined by the intersection of the aluminum 6061 Hugoniot and the second, or reshock, Hugoniot of the powder compact, reflected about the material speed of the first shock state.[24] Although we cannot reconstruct this reshock Hugoniot in detail from our data, it is obvious from Fig. 4 that the locus of reshocked states is qualitatively similar to the principal Hugoniot of the powder and is considerably different from that of the solid. This observation is consistent with a relative density of $\sim$70% behind the initial shock (Tables II and III), for which we expect the reshock Hugoniot to be comparable to, but slightly steeper than, the principal Hugoniot.

The linear compaction rates of the dynamic experiments correspond to the material speeds behind the primary shock waves, and range from 0.3 to 0.6 km/s. These very high values suggest that rate effects may distinguish the stress - density relationships found in dynamic experiments from those determined statically. Such effects, although small, have been noted at compaction rates and stresses that are much smaller than those which obtain in our experiments.[3,6] For stresses greater than a few tenths of a GPa, our experiments suggest that the static stress - density behavior is independent of initial relative density ρ when $\rho < 60\%$. The static compaction of powders having initial relative densities of 47% and 40% should, therefore, be close to that shown in Fig. 5 over the stress range covered by our dynamic experiments. Hence, comparisons between the dynamic and static data obtained here should be representative of the relative compaction rate behavior of these powders.

The dynamic results in Fig. 5 indicate that compaction to a relative density of 65 to 70% occurs readily at stresses below 0.25 GPa, independent of powder type or initial density. This observation is consistent with the

rearrangement stage of powder compaction suggested by Cooper and Eaton[2] and is also apparent in the rapid initial rise of the density with stress seen in the static data. Most of the compaction observed in ceramic powders having initial packing densities below 50% occurs at stresses below 0.3 GPa via this mechanism.[2] At stresses higher than a few tenths of a GPa, however, densification presumably proceeds via fragmentation and plastic flow. Considerable plastic flow is evident in aluminum nitride specimens compacted with explosives to final densities in excess of 90%,[10,11] suggesting that such flow is essential to the formation of dense, well-bonded specimens.

For a powder subjected to a rate of loading P, the density is given in general by:

$$\rho = \rho_r \left(P, \dot{P}^{-1}, t/t_r, t_d/t_r\right) \quad , \tag{4}$$

where the term $\dot{P}^{-1}$ emphasizes that we expect density at stress P to decrease as the rate of loading increases, and does not necessarily imply anything regarding the actual form of Eq. (4). Time t_r is a relaxation time associated with the densification process, t is the time since P was initially applied, and t_d is the duration or time of application of $\dot{P}$. For a shock wave, the loading rate $\dot{P}$ is just $\Delta P/\tau$, where τ is the rise time of the stress at the shock front. In porous materials, a lower limit to τ is given by D/v_s, where v_s is the speed of the compaction shock and D is the particle size.[16]*

---

* Note that through the Hugoniot relationships A-1 and A-2 the density in Eq. (4) can also be written as a function of the linear compaction rate, U_p, rather than P.

When different independent mechanisms of consolidation operate concurrently, the right side of Eq. (4) can be written as a sum:

$$\rho = \rho_a (P, \dot{P}^{-1}, t_d/t_a) + \rho_f (P, \dot{P}^{-1}, t_d/t_f) + \rho_p (P, \dot{P}^{-1}, t_d/t_p) \quad , \quad (5)$$

where ρ_a, ρ_f, and ρ_p are the integrated contributions from rearrangement, fragmentation, and plastic flow, respectively. For convenience of notation the dependence on t has been suppressed. The rate dependence of each mechanism will, in general, be different, and their relative rate sensitivities can be assessed crudely by comparing the characteristic relaxation times, t_a, t_f, and t_p, with the loading time, t_d. If the relaxation times are small relative to t_d, the compact is always in mechanical equilibrium and the effect of loading rate is negligible. However, when t_d is small compared with the relaxation times, mechanical equilibrium cannot be maintained and the effect of loading rate becomes significant. Under static conditions t_d is large and $\dot{P}$ is small so that all mechanisms contribute to the smooth compaction behavior observed as a function of stress. During dynamic compaction the loading time t_d is just the rise time of the compaction shock τ. Depending upon the mechanism, this may be larger or smaller than the characteristic relaxation times. The particle rearrangement stage, for example, is controlled largely by the inertia of the powder particles, particularly at low initial densities. The time to accelerate an individual particle is roughly the time required to propagate a stress wave through it, D/c_0, where c_0 is the sound speed of the solid, here about 10 km/s. Hence, if inertial contributions to rate effects are unimportant we should find that $\tau > D/c_0$, or $v_s < 10$ km/s. For the powders we have studied, v_s varies from 0.7 to 2 km/s, implying that particle rearrangement occurs dynamically much as it does statically, consistent with what we observe (Fig. 5). Presumably the other densification

mechanisms have longer relaxation times relative to τ, yielding lower dynamic densities at higher stresses. If this is so, the transition from the rearrangement stage should become increasingly abrupt as loading rate increases, as the data in Fig. 5 suggest.

Each point on the Hugoniot corresponds to the maximum rate of compaction which can be achieved in a powder of given initial density at a given stress. Hence, the densities derived from the Hugoniots set a lower bound on the possible values which can be obtained as a function of compaction rate. While this bound is approximately constant in the stress range of 0.25 to 1.8 GPa for the powders we have studied, it increases toward the solid density at higher stresses.[10,11,32] We have indicated such behavior schematically in Fig. 5. The work of Hoy et al.[32] on prepressed compacts with initial densities of 67% and 76%, however, indicates that densification is not complete at stresses as high as 6 GPa.

VI. Summary and Conclusions

We have presented a limited number of Hugoniot measurements for two unsintered aluminum nitride powders having initial densities of 1.53 g/cm^3 (47%) and 1.30 g/cm^3 (40%), and have compared them with static data. Dynamic stress - density data calculated from the Hugoniot curves show that the relative density behind the first shock is approximately constant at 70% of the solid. Static compaction measurements, in contrast, show a typical, asymptotic increase of density with stress which varies only slightly for initial densities between 1.79 g/cm^3 (55%) and 1.96 g/cm^3 (60%).

From this work we conclude the following:

1. The initial consolidation of the powder proceeds readily to 70% relative density at stresses below about 0.25 GPa independent of initial density. The mechanism in this stress range, particle rearrangement, is

insensitive to compaction rate.

2. For stresses between 0.25 GPa and 1.8 GPa, densification is dominated by mechanisms that are apparently more sensitive to compaction rate. At the linear compaction rates of our experiments, 0.3 to 0.6 km/s, densities are smaller than corresponding static values and are independent of the stress.
3. Secondary shocks contribute to the final density of the compact when densification behind the primary shock is incomplete.

ACKNOWLEDGMENTS: The authors express their thanks to T. Sullivan for assembling the dynamic experiments, and to E. M. Lilley who performed the static compaction experiments.

Appendix. The Rankine-Hugoniot Relationships and Experimental Details

Given a material at initial stress P_0, material speed U_0, and specific volume V_0, subjected to a discontinuous shock wave. The stress P, material speed U_p, specific volume V behind the shock, and the speed of the shock relative to the unshocked material, v_s, are related by the following conservation relationships:

$$U_p - U_0 = v_s(1 - V/V_0) \qquad \text{(Mass conservation)} \quad . \tag{A-1}$$

$$P - P_0 = v_s(U_p - U_0)\ (1/V_0) \quad \text{(Momentum conservation)} \quad . \tag{A-2}$$

The specific energy deposited in the material behind the shock front is

$$E - E_0 = (P + P_0)\ (V_0 - V)/2 \quad . \tag{A-3}$$

Equations A-1 and A-2 may be combined to give

$$v_s^2 = V_0(P - P_0)/(1 - V/V_0) \quad . \tag{A-4}$$

In fact, for these relationships to be valid, it is sufficient that the wave be steady, i.e., that it travel at constant velocity without changes in shape. That the wave velocity is constant in dynamically loaded porous metals was demonstrated by Boade for copper[28,29] and tungsten[33] and by Lysne and Halpin for iron.[34] Although Lysne and Halpin report some apparent changes in amplitude with propagation distance in porous iron, Boade[28] finds no such effect in porous copper. This result and the constancy of the shock speeds suggest that the Hugoniot relationships can be applied to the compaction wave. It is significant to note in this regard that good agreement is obtained between experimental data obtained in this way and a theoretical analysis based on Hugoniot theory in the regime of complete densification of the porous body.[27,30,31,35] In using Eqs. A-1 through A-4 we have made the

assumption that AlN powder behaves in the same way as metal powders. While this is reasonable, we hasten to point out that we have no direct evidence for its validity. Wave propagation studies as a function of thickness are required, but were beyond the scope of our work.

The utility of the impedence matching method of Hugoniot determination requires that the Hugoniot of the projectile, in this case Al 6061-T6, be well known. In fact, for our experiments, in which the shock produced in the cover plate by the projectile actually releases into the lower-impedance powder, we properly should use the isentrope. At the low stresses produced in the aluminum in our experiments, however, the isentrope and the Hugoniot are very close and the use of the Hugoniot is an excellent approximation. The Hugoniot of Al 6061-T6 is, unfortunately, somewhat complicated. This material has a Hugoniot elastic limit at approximately 0.41 GPa (4.1 kbar) which produces an elastic precursor of this amplitude.[36,37] This precursor travels faster[36] than the larger-amplitude plastic wave, and it impinges on the powder about 80 ns earlier in the experiments at the lowest stresses. Hence the initial loading of the powder is accomplished by a complex series of interactions between two waves. For the highly distended powders we have studied, however, it is clear from the Hugoniot data in Fig. 4 that the stress wave induced in the powder by the precursor is of very small amplitude and has a correspondingly small propagation velocity. Although it is very difficult to determine with any certainty, we estimate that the wave speed for the hypothetical precursor in the powder is 0.1-0.2 km/s. For the slowest measured compaction wave speed of 0.7 km/s (experiment 155), it follows that the main compaction wave will catch the precursor and form a single shock ("shock-up") after 13-32 ns, corresponding to 0.9-2.2 X 10^{-3} cm. The shock-up time and distance will decrease as the amplitude of the compacting shock and its velocity increase. The shock-up distance is considerably less

than the sensor thickness (1.27×10^{-2} cm), a major source of systematic error. Hence we assume that additional error from the elastic precursor in the aluminum is negligible. For similar reasons, the rate-dependent "plastic" precursor effect discussed by Wallace[36] and the details of the unloading in the aluminum cover are not deemed important for our experiments. Our arguments follow directly from the great difference in acoustic impedance between the solid aluminum and the highly distended powder as well as the rapid relative increase in wave velocity in the powder with stress. Obviously, if the wave velocities in the cover and specimen were comparable, the presence of precursors and rate effects would take on greater importance.

The Hugoniot we have used for Al 6061-T6 is derived from high-pressure data and is described by the shock velocity - material velocity relationship:

$$v_{Al} = 5.35 + 1.34U_p \text{ km/s} \quad . \tag{A-5}$$

This was derived from data obtained at stresses in excess of 7.0 GPa,[17] and when extrapolated to low stresses does not properly describe the details of the elastic response. Wallace,[36] however, notes that a relationship similar to Eq. (A-5) provides an adequate description of the plastic wave speeds at low stresses as well. A comparison of the proper aluminum Hugoniot with a Hugoniot elastic limit of 0.41 GPa and a material speed of 0.023 km/s with that used in the analysis (Fig. 4) shows that the two are barely distinguished. In practical terms, then, Eq. (A-5) is adequate for these experiments.

Random uncertainties in the experiments were handled in the usual manner. The acoustic impedance is given by

$$Z_{pow} = \rho_0 v_s = v_s/V_0 \quad , \tag{A-6}$$

and the measured shock speed by

$$v_s = \delta/\Delta t \quad , \tag{A-7}$$

where δ is the measured powder thickness and Δt the shock transit time. Defining the uncertainties in these quantities and the powder density as $s(\delta)$, $s(\Delta t)$, and $s(\rho_0)$, it follows that the associated random uncertainties in Z_{pow} and v_s are

$$s(Z_{pow}) = \sqrt{[v_s s(\rho_0)]^2 + [\rho_0 s(v_s)]^2} \tag{A-8}$$

and

$$s(v)_s = \sqrt{\left(\frac{s(\delta)}{\Delta t}\right)^2 + \left(\frac{\delta s(\Delta t)}{(\Delta t)^2}\right)^2} \quad . \tag{A-9}$$

Notice that, unlike solids, the uncertainty in the specimen density contributes to the overall uncertainty. The impedance matched stress and material speed are given by

$$P = \frac{U_{proj}}{\frac{1}{Z_{pow}} + \frac{1}{Z_{proj}}} \tag{A-10}$$

and

$$U_p = \frac{U_{proj}}{1 + \frac{Z_{pow}}{Z_{proj}}} \quad , \tag{A-11}$$

where U_{proj} is the measured projectile speed and Z_{proj} is the acoustic impedance of the projectile. Assuming no random uncertainty in Z_{proj} and defining $\zeta = 1 + Z_{pow}/Z_{proj}$, the random uncertainties in the stress and material speed are

$$s(P) = \sqrt{\left[\frac{s(U_{proj})}{\frac{1}{Z_{pow}} + \frac{1}{Z_{proj}}}\right]^2 + \left[\frac{U_{proj}\, s(Z_{pow})}{\zeta^2}\right]^2} \qquad \text{(A-12)}$$

and

$$s(U_p) = \sqrt{\left[\frac{s(U_{proj})}{\zeta}\right]^2 + \left[\frac{U_{proj}\, s(Z_{pow})}{Z_{proj}\, \zeta^2}\right]^2} \; . \qquad \text{(A-13)}$$

The uncertainties in the density and projectile speed were estimated from the averaged square deviation from the mean (the variance). The square root of the variance is an estimator for the standard deviation of a normally distributed random variable, corresponding to 67% confidence. We report at the 95% confidence level, given at two standard deviations, so that here $s(U_{proj}) = 2\sqrt{Var(U_{proj})}$ and $s(\rho_0) = 2\sqrt{Var(\rho_0)}$. Generally, $Var(U_{proj})/U_{proj}$ was 1-2% and $Var(\rho_0)$ was approximately 0.01 g/cm^3. $s(\delta)$ and $s(\Delta t)$ were estimated to be 2.54 X 10^{-3} cm and 10 ns, respectively. Random uncertainties are shown with error bars in Fig. 4.

Systematic errors are more difficult to estimate. The dominant source of systematic error is the relatively large thickness of the carbon sensors and the associated long rise time (100-200 ns). This error significantly affects both the transit time and the powder thickness to be used in calculating the shock velocity, Eq. (A-7). We chose δ to be the distance between the midpoints of the sensors and Δt to be the time between the trigger levels

(2 volts) on the front and rear sensor signals. This approach, which is somewhat arbitrary, has nevertheless been successfully used for metal powders[27] that compact to near-solid density. Under conditions of complete compaction, the stress, volume, and material speed of the final state can be predicted independent of the details of the powder collapse. The agreement of the experimental data[27] with such predictions indicates that the systematic errors are not large. We assume this is true for AlN as well.

Figure Captions

Fig. 1. Schematic illustration of the sample assembly. The aluminum cover plate was supported on three piezoelectric pins placed symmetrically around its perimeter. Signals from these pins provide a determination of the relative tilt at impact of the projectile and the cover. The thickness of the carbon sensors has been exaggerated for clarity. Their actual thickness at the carbon element is 0.0125 cm. The container was fabricated from 304 stainless steel.

Fig. 2. Scanning electron micrograph of particles of powder I. The powder particles consist of aggregates of 0.1-μm crystallites. The powder has been dispersed on a backing material to facilitate observation.

Fig. 3. Carbon sensor records for aluminum nitride, shot 140 (Table II): (a) front sensor record, showing the stress in the compact behind the initial shock and the much larger stress from the reflection that returns from the back of the assembly. The amplitude of this reflected pulse is somewhat higher than the stress recorded at the rear sensor (b) because of the difference in shock impedance, ρv_s, between the AlN powder and the aluminum plates on either side (Fig. 1) (see Ref. 24).

Fig. 4. Hugoniot curves of aluminum nitride powders having initial densities 1.53 g/cm^3 (powder I) (a) and 1.30 g/cm^3 (powder II) (b). Unmarked data points are derived from impedance matching. Those marked with a "G" are direct sensor readings which have been corrected for sensor errors if the stress is greater than 2.0 GPa (Ref. 27). The dashed curves were calculated assuming the linear compaction relationship, Eq. (3). The dotted curves were calculated assuming that the powder crushes to solid density immediately upon the application of a stress, regardless of its magnitude. Reshock states on the Hugoniot of solid aluminum 6061 are indicated with an "R." The Hugoniot of solid AlN is included for reference.

Fig. 5. Relative density as a function of the stress. Data points are calculated from the impedance-match Hugoniot data and represent values at stress. The solid curve is calculated from the relationship $\rho_r = 0.685 + 0.017P$ (GPa) and the dotted curves are hypothetical behavior at low and high stresses. The dashed curves are static data obtained for powders having initial relative densities of 55% and 60% (see text).

References

[1]R. A. Thompson, "Mechanics of Powder Pressing: I, Model for Powder Densification; II, Finite-Element Analysis of End-Capping in Pressed Green Powders; III, Model for the Green Strength of Pressed Powders," Am. Ceram. Soc. Bull. 60(2), 237-251 (1981).

[2]A. R. Cooper, Jr., and L. E. Eaton, "Compaction Behavior of Several Ceramic Powders," J. Am. Ceram. Soc. 45(3), 97-101 (1962).

[3]D. B. Leiser and O. J. Whittemore, Jr., "Compaction Behavior of Ceramic Particles," Am. Ceram. Soc. Bull. 49(8), 714-717 (1970).

[4]O. J. Whittemore, Jr., "Particle Compaction," in Ceramic Processing Before Firing, G. Y. Onoda, Jr., and L. L. Hench, eds., Wiley, New York, 1978, pp. 343-355.

[5]S. J. Lukasiewicz and J. S. Reed, "Character and Compaction Response of Spray-Dried Agglomerates," Am. Ceram. Soc. Bull. 57(9), 798-805 (1978).

[6]R. A. Youshaw and J. W. Halloran, "Compaction of Spray-Dried Powders," Am. Ceram. Soc. Bull. 61(2), 227-230 (1982).

[7]R. Prummer and G. Ziegler, "Strukturelle Änderungen beim Explosivkompaktieren von Aluminiumoxidpulvern," Ber. Dt. Keram. Ges. 51, 343-347 (1974).

[8]R. Prummer, "Die Verdichtung von Keramik - und Metallpulvern sowie deren Mischungen durch Explosivdrück," Ber. Dt. Keram. Ges. 50, 75-81 (1973).

[9]C. L. Hoenig and C. S. Yust, "Explosive Compaction of AlN, Amorphous Si_3N_4, Boron, and Al_2O_3 Ceramics," Am. Ceram. Soc. Bull. 60(11), 1175-1224 (1981).

[10]W. H. Gourdin, C. J. Echer, C. F. Cline and L. E. Tanner, "Microstructure of Explosively Compacted Aluminum Nitride Ceramic," pp. 233-241 in Proc. 7th International Conference on High Energy Rate Fabrication, T. Z. Blazynski, ed., University of Leeds, 1981.

[11]W. H. Gourdin, S. L. Weinland, C. J. Echer and S. L. Huffsmith, "Explosive Consolidation of Aluminum Nitride Ceramic Powder: A Case History," pp. 657-671 in Emergent Process Methods for High Technology Ceramics, R. F. Davis, H. Palmour III, and R. L. Porter, eds., Plenum, New York, 1984.

[12]M. Mitomo and N. Setaka, "Consolidation of Si_3N_4 by Shock Compression," J. Mat. Sci. 16(3), 851-852 (1981).

[13]T. Akashi, A. Sawaoka, S. Saito and M. Araki, "Structural Changes of Boron Nitride Caused by Multiple Shock-Compressions," Japan J. Appl. Phys. 15(5), 891-892 (1976).

[14]T. Sato, T. Ishii and N. Setaka, "Formation of Cubic Boron Nitride from Rhombohedral Boron Nitride by Explosive Shock Compression," Comm. Am. Ceram. Soc., Oct. 1982, p. C-162.

[15]N. Setaka and Y. Sekikawa, "Diamond Synthesis from Carbon Precursor by Explosive Shock Compression," J. Mat. Sci., 16(6), 1728-1730 (1981).

[16]W. H. Gourdin, "Energy Deposition and Microstructural Modification in Dynamically Consolidated Metal Powders," J. Appl. Phys. 55(1), 172-181 (1984).

[17]S. P. Marsh, ed., LASL Shock Hugoniot Data, University of California Press, Berkeley, 1980.

[18]S. W. Kieffer, "Shock Metamorphism of the Coconino Sandstone at Meteor Crater, Arizona," J. Geophys. Res. 76(23), 5449-5473 (1971).

[19]P. C. Lysne, "A Comparison of Calculated and Measured Low-Stress Hugoniots and Release Adiabats of Dry and Water-Saturated Tuff," J. Geophys. Res. 75(23), 4375-4386 (1970).

[20]R. F. Trunin, G. V. Simakov and M. A. Podurets, "Shock-wave Compression of Porous Rutile," Earth Physics 12, 13-18 (1974) [Iz. Nauk. USSR 12, 789-792 (1974)].

[21]V. S. Trofimov, G. A. Adadurov, S. V. Pershin and A. N. Dremin, "Anomalous Shock Compressibility of Porous Materials," Combustion, Explosion, and Shock Waves 4(2), 142-147 (1968). [Fizika Goreniya i Vzryva 4, 244-253 (1968)].

[22]D. C. Erlich and D. R. Curran, "Characterization of the Dynamic Behavior of Porous Solids, Part 6: Dynamic Response of Porous Ceramics - Experiments," Report DNA 3961 F-6, Stanford Research Institute, Menlo Park, CA, 1976; see also L. Seaman, R. E. Tokheim and D. R. Curran, "Computational Representation of Constitutive Relations for Porous Materials," Report DNA 3412F, Stanford Research Institute, Menlo Park, CA, 1974, p 88.

[23]H. C. Heard and C. F. Cline, "Mechanical Behavior of Polycrystalline BeO, Al_2O_3, and AlN at High Pressure," J. Mat. Sci. 15(8), 1889-1897 (1980).

[24]See, for example, G. E. Duvall and G. R. Fowles, "Shock Waves," in High Pressure Physics and Chemistry, Volume 2, R. S. Bradley, ed., Academic Press, London, 1963, pp. 222-223; D. B. Hayes, "Introduction to Stress Wave Phenomena," Report SLA-73-0801, Sandia National Laboratories, Albuquerque, NM, August 1973.

[25]D. R. Stephens, E. M. Lilley and H. Louis, "Pressure-volume Equation of State of Consolidated and Fractured Rocks to 40 kbar," Inter. J. Rock Mech. and Mining Sci. 7(3), 257-267 (1970).

[26]R. R. Horning and W. M. Isbell, "Behavior of Porous Beryllium under Thermomechanical Loading, Part 7: Calibration Studies on the Carbon Pizoresistive Gage," University of California, Lawrence Livermore National Laboratory Report UCRL-51682, Pt. 7, June 17, 1975.

[27]W. H. Gourdin and S. L. Weinland, "Hugoniot Measurements on Unsintered Metal Powders," in Shock Waves in Condensed Matter - 1983, J. R. Asay, G. K. Straub and R. A. Graham, eds., North Holland, New York, 1984, pp. 99-102.

[28]R. R. Boade, "Principal Hugoniot, Second-Shock Hugoniot, and Release Behavior of Pressed Copper Powder," J. Appl. Phys. 41(11), 4542-4551 (1970).

[29]R. R. Boade, "Compression of Porous Copper by Shock Waves," J. Appl. Phys. 36, 5693-5702 (1968).

[30]W. Herrmann, "Constitutive Equation for the Dynamic Compaction of Ductile Porous Materials," J. Appl. Phys. 40(6), 2490-2499 (1969).

[31]M. M. Carroll and A. C. Holt, "Suggested Modification of the P-alpha Model for Porous Materials," J. Appl. Phys. 43(2), 759-761 (1972).

[32]D. E. P. Hoy, M. Akaishi, J. K. Park, Y. Horie and J. K. Whitfield, "Shock Compression of Aluminum Nitride Powder," in Shock Waves in Condensed Matter - 1983, J. R. Asay, G. K. Stroub and R. A. Graham, editors, North Holland, New York, 1984, pp. 451-454.

[33]R. R. Boade, "Dynamic Compression of Porous Tungsten," J. Appl. Phys. 40, 3781-3785 (1969).

[34]P. C. Lysne and W. J. Halpin, "Shock Compression of Porous Iron in the Region of Incomplete Compaction," J. Appl. Phys. 39, 5488-5495 (1968).

[35]B. M. Butcher and C. H. Karnes, "Dynamic Compaction of Porous Iron," J. Appl. Phys. 40, 2967-2976 (1969).

[36]D. C. Wallace, "Flow Process of Weak Shocks in Solids," Phys. Rev. B 22(4) 1487-1494 (1980).

[37]J. N. Johnson and L. M. Barker, "Dislocation Dynamics and Steady Plastic Wave Profiles in 6061-T6 Aluminum," J. Appl. Phys. 40(11), 4321-4334 (1969).

Table I. Powder Characteristics

Characteristic	Powder I*	Powder II**
Composition (wt%)	93.0 AlN 4.2 $Al_2O_3^{\dagger}$ 2.0 Free Al 0.06 C	96.0 AlN 3.0 $Al_2O_3^{\dagger}$ 1.0 Free Al
Particle size range (μm)	1-20	1-7
Median particle size (weight basis--μm)	6	2.5
ACP ("solid") density (g/cm^3)††	3.2	3.2
Packing density (g/cm^3)	1.53	1.30
Surface area (m^2/g)	3.4	3.4

* Materials Research Corporation, Orangeburg, NY.

** Cerac/Pure Inc., Milwaukee, WI, lot number A1120.

† The Al_2O_3 content is obtained by subtraction of the AlN and free Al assays from the total assay of Al in the specimen.

†† Air comparison pycnometer.

Table II. Shock Results for Powder of Initial Density 1.53 g/cm^3

Expt.	Type*	Projectile speed (km/s)	Stress (GPa)	Material speed (km/s)	V (cm^3/g)	Relative density at stress**
Primary Shock						
144	Imp.	0.312	0.41	0.184	0.4557	0.67
	G	0.312	0.34	0.289	0.4079	0.75
142	Imp.	0.427	0.65	0.382	0.4293	0.71
	G	0.427	0.61	0.386	0.4073	0.75
143	Imp.	0.518	0.95	0.453	0.4366	0.71
140	Imp.	0.591	1.17	0.512	0.4283	0.71
	G	0.591	1.07	0.518	0.4028	0.76
145	Imp.	0.652	1.39	0.558	0.4293	0.71
146	Imp.	0.738	1.76	0.620	0.4344	0.70
Reshock						
144	G		1.33	0.090	0.4147	0.74
142	G		1.85	0.124	0.3732	0.82
143	CG		2.3	0.153	0.3698	0.83
140	CG		2.8	0.185	0.3629	0.84
145	CG		3.2	0.210	0.3623	0.85

* Imp. = impedance matching: G = direct sensor measurement; CG = corrected sensor measurement.

** Relative to the solid density at atmospheric pressure, 3.26 g/cm^3.

Table III. Shock Results for Powder of Initial Density 1.30 g/cm^3

Expt.	Type*	Projectile speed (km/s)	Stress (GPa)	Material speed (km/s)	V (cm^3/g)	Relative density at stress**
Primary Shock						
155	Imp.	0.323	0.268	0.305	0.4229	0.73
	G	0.323	0.280	0.304	0.4397	0.70
137	Imp.	0.449	0.508	0.414	0.4318	0.71
153	Imp.	0.599	0.994	0.531	0.4851	0.63
	G	0.599	0.98	0.532	0.4801	0.64
152	Imp.	0.749	1.268	0.663	0.4224	0.68
Reshock						
137	CG		2.0	0.134	0.3791	0.81
153	CG		2.8	0.185	0.4187	0.73
152	CG		3.9	0.254	0.3587	0.86

* Imp. = impedance matching: G = direct sensor measurement; CG = corrected sensor measurement.

** Relative to the solid density at atmospheric pressure, 3.26 g/cm^3.

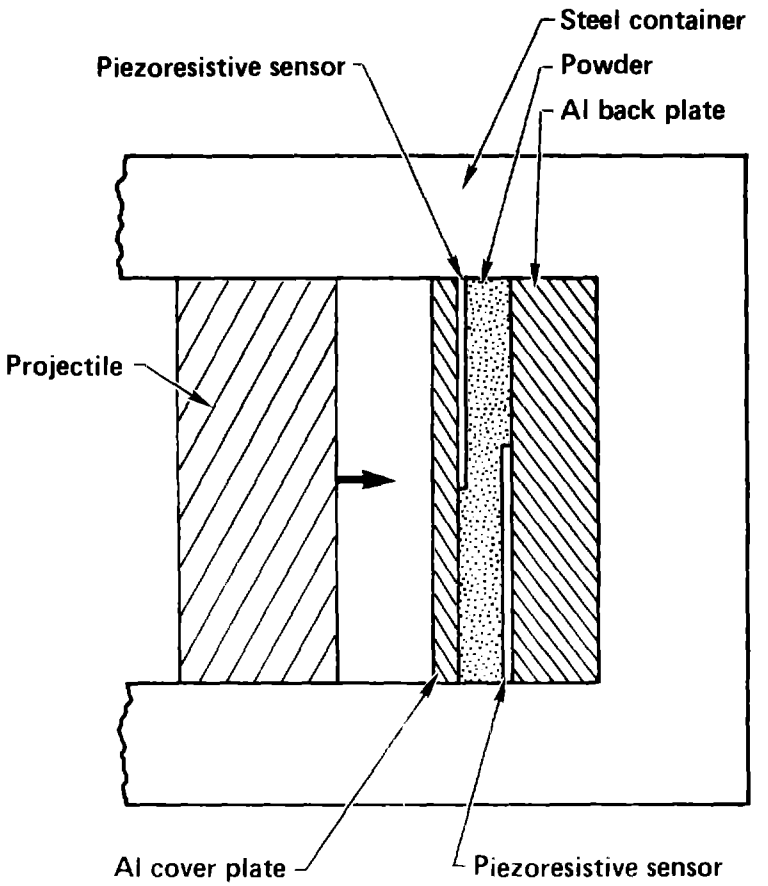
Steel container
Piezoresistive sensor
Powder
Al back plate
Projectile
Al cover plate
Piezoresistive sensor

Figure 1

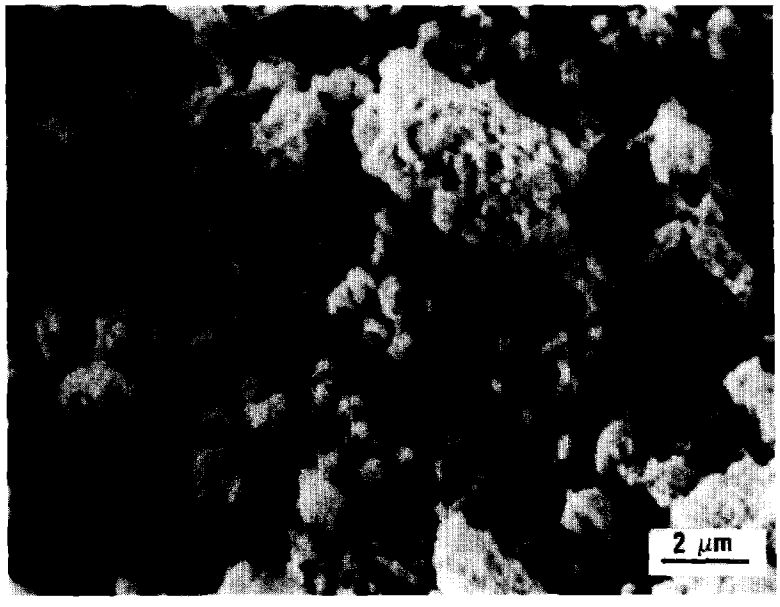

Figure 2

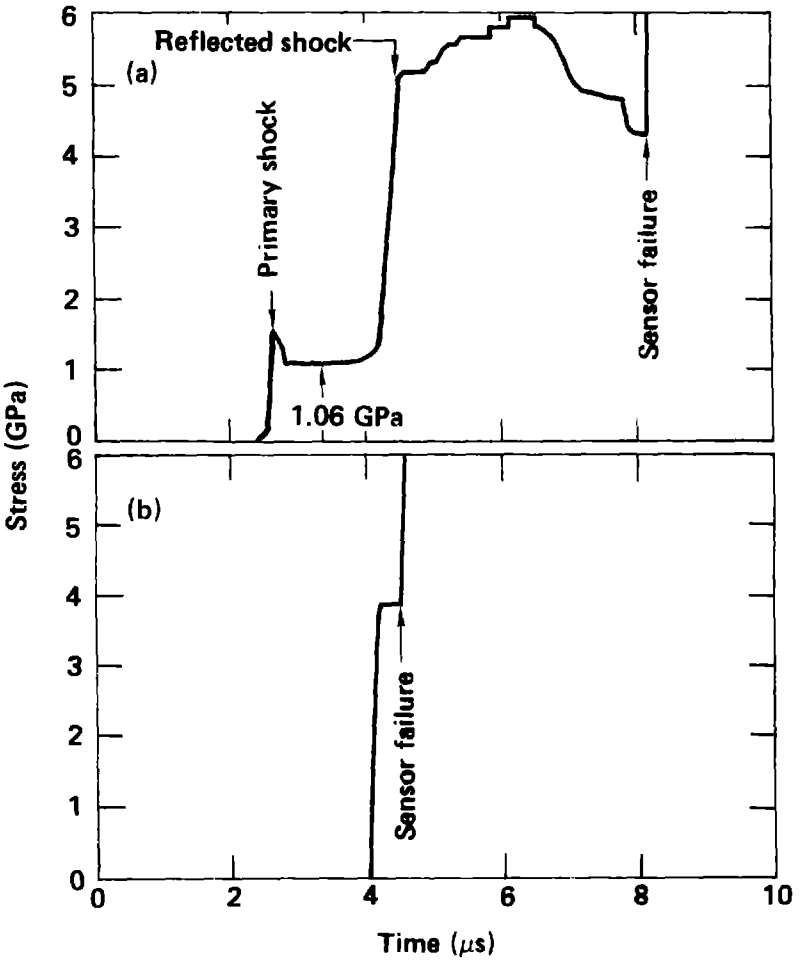
Reflected shock
(a)
Primary shock
1.06 GPa
Sensor failure
(b)
Sensor failure
Stress (GPa)
Time (μs)
0
1
2
3
4
5
6
0
2
4
6
8
10

Figure 3

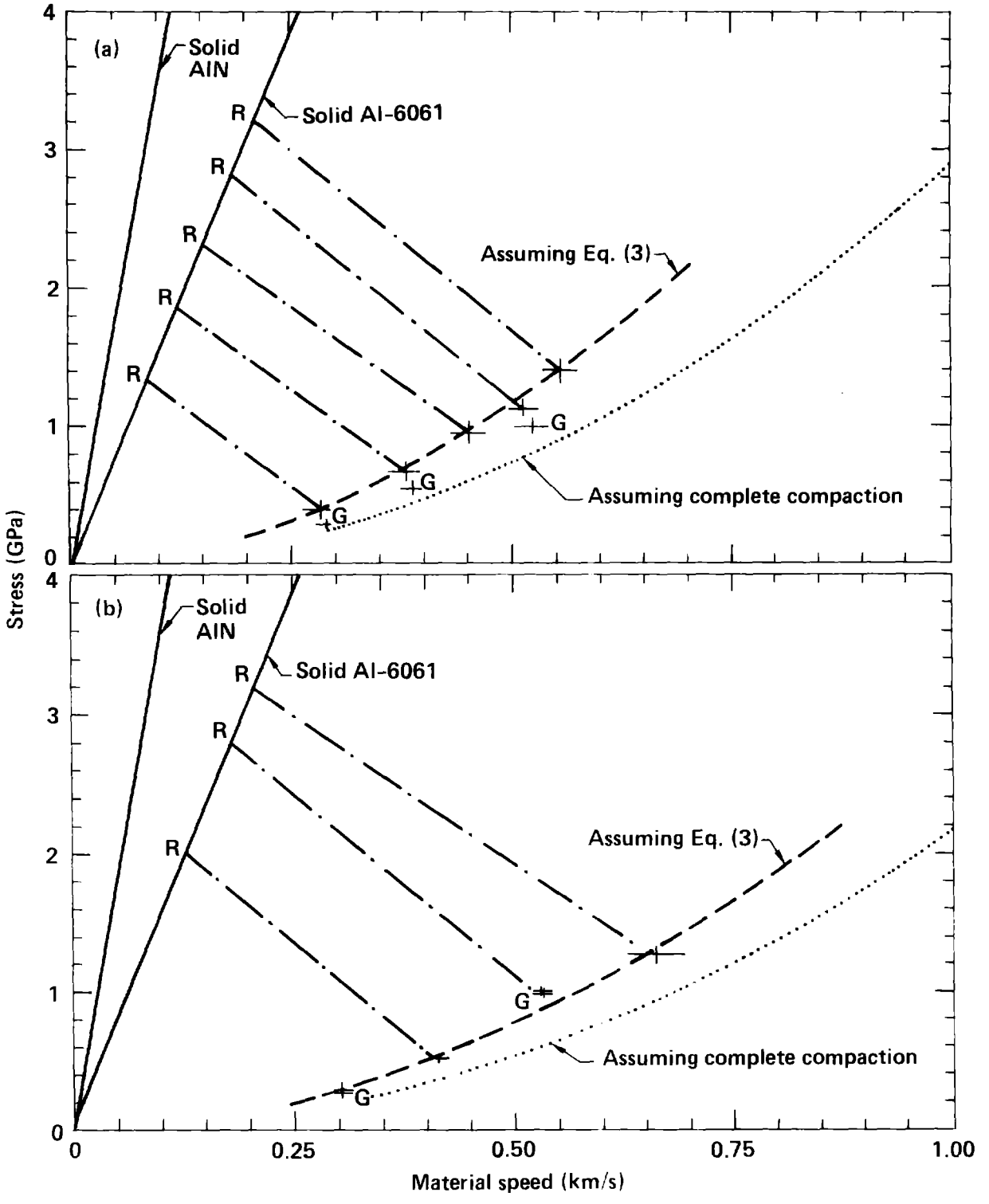
(a)
Solid AlN
Solid Al-6061
R
G
Assuming Eq. (3)
Assuming complete compaction
(b)
Stress (GPa)
Material speed (km/s)
0
0.25
0.50
0.75
1.00
1
2
3
4

Figure 4

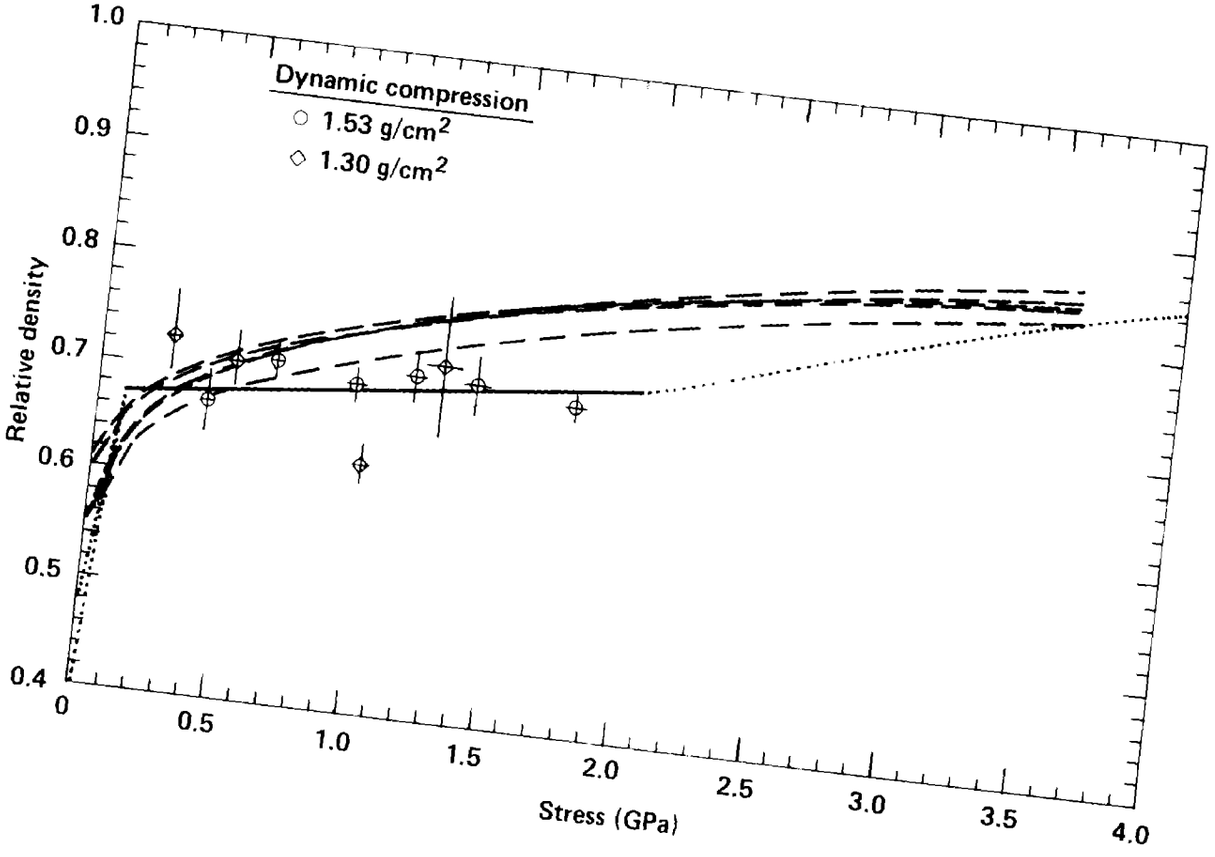
Dynamic compression
1.53 g/cm2
1.30 g/cm2
Relative density
1.0
0.9
0.8
0.7
0.6
0.5
0.4
0
0.5
1.0
1.5
2.0
2.5
3.0
3.5
4.0
Stress (GPa)

Figure 5